BNL-107758-2015-JA

Atomic-resolution 3D structure of amyloid β fibrils: the Osaka mutation

Anne K. Schütz,[1] Toni Vagt,[2] Matthias Huber,[1] Oxana Y. Ovchinnikova,[2] Riccardo Cadalbert,[1] Joseph Wall,[3] Peter Güntert,[4] Anja Böckmann,[5] Rudi Glockshuber,[2] and Beat H. Meier[1]

[1]Physical Chemistry, ETH Zurich, Wolfgang-Pauli-Strasse 10, CH-8093 Zurich, Switzerland
[2]Institute of Molecular Biology and Biophysics, ETH Zurich, Schafmattstrasse 20, CH-8093 Zurich, Switzerland
[3]Brookhaven National Laboratory, 50 Bell Avenue, Building 463, Upton, NY 11973-5000, USA
[4]Institute of Biophysical Chemistry, Center for Biomolecular Magnetic Resonance, and Frankfurt Institute for Advanced Studies, Goethe University, Frankfurt am Main, Germany
[5]Institut de Biologie et Chimie des Proteines, UMR 5086 CNRS/ Universite de Lyon 1, 7 passage du Vercors, 69367 Lyon, France

Submitted to Angewandte Chemie International Edition

August 2014

Biological, Environmental & Climate Sciences Department
Brookhaven National Laboratory

U.S. Department of Energy
Office of Science
Office of Biological and Environmental Research

Notice: This manuscript has been authored by employees of Brookhaven Science Associates, LLC under Contract No. DE-AC02-98CH10886 with the U.S. Department of Energy. The publisher by accepting the manuscript for publication acknowledges that the United States Government retains a non-exclusive, paid-up, irrevocable, world-wide license to publish or reproduce the published form of this manuscript, or allow others to do so, for United States Government purposes.

DISCLAIMER

This report was prepared as an account of work sponsored by an agency of the United States Government. Neither the United States Government nor any agency thereof, nor any of their employees, nor any of their contractors, subcontractors, or their employees, makes any warranty, express or implied, or assumes any legal liability or responsibility for the accuracy, completeness, or any third party's use or the results of such use of any information, apparatus, product, or process disclosed, or represents that its use would not infringe privately owned rights. Reference herein to any specific commercial product, process, or service by trade name, trademark, manufacturer, or otherwise, does not necessarily constitute or imply its endorsement, recommendation, or favoring by the United States Government or any agency thereof or its contractors or subcontractors. The views and opinions of authors expressed herein do not necessarily state or reflect those of the United States Government or any agency thereof.

Atomic-resolution 3D structure of amyloid β fibrils: the Osaka mutation

Anne K. Schütz[1#], Toni Vagt[2#], Matthias Huber[1], Oxana Y. Ovchinnikova[2], Riccardo Cadalbert[1], Joseph Wall[3], Peter Güntert[4], Anja Böckmann[5*], Rudi Glockshuber[2*] and Beat H. Meier[1*]

[1]*Physical Chemistry, ETH Zürich, Wolfgang-Pauli-Strasse 10, CH-8093 Zurich, Switzerland*
[2]*Institute of Molecular Biology and Biophysics, ETH Zurich, Schafmattstrasse 20, CH- 8093 Zurich, Switzerland*
[3]*Brookhaven National Laboratory, 50 Bell Avenue, Building 463,Upton, NY 11973-5000, USA*
[4]*Institute of Biophysical Chemistry, Center for Biomolecular Magnetic Resonance, and Frankfurt Institute for Advanced Studies, Goethe University, Frankfurt am Main, Germany*
[5]*Institut de Biologie et Chimie des Protéines, UMR 5086 CNRS/Université de Lyon 1, 7 passage du Vercors, 69367 Lyon, France*

*Corresponding authors:
Beat H. Meier (beme@ethz.ch), Rudi Glockshuber (rudi@mol.biol.ethz.ch)
Anja Böckmann (a.bockmann@ibcp.fr)

[#] these authors contributed equally to this work

Author contributions: RG and BHM conceived the study, AKS, TV, OO and RC produced samples, AKS obtained the distant-restraint NMR spectra, AKS, MH, AB, BHM analyzed the data, JW performed and analysed MPL measurments. PG supported the structure calculations, AKS, AB and BHM wrote the paper and all authors were involved into the editing.

Alzheimer's disease (AD) is a progressive neurodegenerative disorder that constitutes the most common cause of dementia. AD is accompanied by deposits of amyloid β-peptide (Aβ) in extracellular proteinaceous plaques in the brain[1]. In the amyloid cascade hypothesis[2], the formation of Aβ oligomers and fibrils is suspected to be the key event in the development of AD. To further develop the link between Aβ and AD, 3D structures of the different species involved in the disease are necessary. Here, we report an atomic-resolution structure of the Aβ1-40 peptide with the Osaka mutation (E22Δ) in its fibrillar amyloid form. The E22Δ mutation is associated with familial early-onset AD[3]. The fold, which represents a new motif, is based on solid-state NMR data that establish, per monomer, 31 structurally meaningful distance restraints supported by 48 spectrally unambiguous NMR peaks, which can be, also unambiguously, divided in 26 intra- and 22 intermolecular contacts. In addition, 56 dihedral angle restraints and 19 hydrogen bonds, both based on chemical shifts, are entered. For the final structure determination, 2356 additional automatically assigned medium- and long-range cross peaks were taken into account. Contrary to previously proposed models for Aβ, monomers in Aβ1-40 E22Δ fibrils do not assume a simple β-sheet-turn-β-sheet topology, but the fibrils consist of two interlaced molecules per β-sheet layer in a symmetrical arrangement.

Despite its central importance for understanding the molecular basis of Alzheimer's disease, high-resolution structural information on Aβ aggregates is scarce because standard methods, in particular x-ray diffraction and solution-state NMR, cannot be employed to investigate fibrillar aggregates at atomic resolution. Solid-state NMR, in contrast, has demonstrated its potential to yield structures of amyloids fibrils at a

highly resolved level[4-6]. Several structural models for Aβ have been proposed based on solid-state NMR restraints[7-15], the most recent, seeded by a homogenate from diseased brain, representing a beta-hairpin in a trimeric arrangement[15]. They share a common cross-β architecture mostly with in-register parallel pleated sheets[16] and provide strong evidence for polymorphism, namely indicating that the Aβ peptide can exist in a number of different fibril architectures possibly corresponding to different phenotypes of the disease[15], as also postulated for other neurodegenerative diseases[17,18].

Here we combine solid-state NMR and electron microscopy to obtain the atomic resolution structure of amyloid fibrils of Aβ1-40 with the Osaka mutation E22Δ, where glutamate 22 is deleted. Aβ1-40 E22Δ is, in rat primary neuron cultures, more neurotoxic than the wild-type protein and aggregates more readily in *vitro* to form fibrillar bundles with an unusually high thioflavin T binding capacity[19,20]. Combining mass-per-length data from scanning-transmission electron microscopy (STEM) and manually identified unambiguous NMR restraints, we obtain the overall fold of the monomer, as well as the tertiary and quaternary contacts in the fibrils. In a second calculation based on this data and complemented by 631 automatically assigned medium-, long-range and intermolecular NMR distance restraints per monomer, supported by 2356 peaks in the different spectra we obtain an atomic-resolution structural model of Aβ1-40 E22Δ.

The fibril is built by two symmetry-equivalent rigid molecules per layer

While fibrils of Aβ1-40 E22Δ are known to form dense tangles[19], isolated fibril segments suited for scanning transmission-electron microscopy (STEM) can be obtained at an early stage of in *vitro* fibrillization, as shown in Fig. 1a,b. The

experimental mass-per-length (MPL) distribution is plotted in Fig. 1c and reveals that the elementary fibril consists of two molecules for each layer of β-sheet in the amyloid. NMR sequential resonance assignment forming the basis for structure calculation was achieved using a set of 3D experiments and is described in detail in an assignment note[21]. The spectra used for structure determination were recorded on virtually pure samples of a single polymorph. Extracts from NCA an NCO correlation spectra, shown in black in Fig. 1d,e, and from a C-C DARR correlation spectrum in Extended Data Fig. 1, show a single set of resonances per residue, demonstrating that all monomers are symmetry-equivalent. All 39 residues are detected in the spectrum indicating the absence of highly dynamic segments. Together with the STEM data, this observation suggest the presence of one symmetric dimer per layer of the cross-β fibril. Even if two is predominant, we do not exclude a MPL of three on the sole basis of the STEM data, since the relative abundance of 2 versus 3 cannot be quantitatively measured in the tangles. We thus will come back to this point below when calculating structures.

Structural restraints from the spectra

The structure calculation procedure follows established NMR strategies, namely measuring a large number of interatomic distances and converting them into upper distance restraints for triangulation[22]. The distance restraints were extracted from cross peaks in two-dimensional CHHC, PAR, PAIN, DARR and PDSD spectra[23-27] (Fig. 1d,e, 2a,b and in Extended Data Fig. 2,3). As demonstrated earlier for the HET-s prion domain, a relatively small number of spectrally unambiguous (i.e. the two frequencies are reliably assignable to a single atom pair) long-range restraints can already define the structure reasonably well[4], while using the complete information

from all ambiguous and unambiguous cross peaks allows to obtain a more precise structure[5]. We followed a similar scheme here.

For amyloids, structurally meaningful intermolecular distances are abundant and can be of similar length when compared to intramolecular ones[5]. It is therefore necessary to establish the inter- or intramolecular nature using samples with specific isotope labeling patterns.

We first address the question of the register of β-strand stacking into sheets; the observation of highly similar N-Cα and N-C' cross signals (Fig. 1d,e) in NCA/NCO spectra recorded on a uniformly labeled sample (where correlations are of intra-residue nature) and PAIN spectra recorded on a 1:1 mixed [^{15}N]:[^{13}C]-labeled sample (where they exclusively arise from intermolecular interactions between adjacent layers of β-sheet) reveals a parallel in-register stacking of the β-sheets.

Then we look for further peaks that are clearly intermolecular; PAIN spectra of the mixed sample feature only intermolecular ^{15}N-^{13}C correlations and we find strong signals which are not explained by register contacts (examples marked by red crosses in Fig.1d,e). Five of these additional peaks provide spectrally unambiguous intermolecular restraints (listed in Extended Data Table 1) for the following residue pairs: Glu3-Gly29, His13-Val40 (two restraints), Gln15-Gly37, and Gln15-Gly38. Some of them even stronger than the register contacts given in the blue PAIN spectrum of Fig 1f,g, recorded on the uniformly labeled sample, suggesting that the corresponding intermolecular contact tends to be shorter than the β-sheet register distance of ~4.8 Å.

Further information about intra- and intermolecular packing was obtained by comparing the cross-peak intensity between uniformly labeled and dilute labeled

samples (labeled monomers diluted in unlabeled ones) in CHHC, PAR and DARR spectra (Fig. 2a,b,d and Extended Data Fig. 4). In these spectra intermolecular peaks must be attenuated by roughly the dilution ratio (here 1:4), while intramolecular peaks remain constant. A detailed comparison of the diluted and ndilluted spectra is given ih Extended Data Fig.4 and the resulting attenuation factors are given in Fig. 2c and Extended Data Fig.5 Their analysis yielded peaks that are not only spectrally unambiguous but that represent unambiguously intermolecular restraints between residues Glu3-Lys28, Glu3-Gly29, Glu3-Ala30, His13-Val40 and unambiguously intramolecular ones between His6-Glu11, His6-His13, Phe19-Leu34, Phe20-Ile31, Ile32-Met35, Met35-Gly38. Together with the 5 restraints from PAIN spectra, a total of 48 spectrally unambiguous restraints were thus extracted from the spectra and classified into 22 intermolecular and 26 intramolecular restraints (Extended Data Table 1 and Fig. 3a). Thus 'unambiguous' here refers to both spectrally unambiguous, as well as unambiguous with respect to the classification inter-/intermolecular.

Structure calculation of the Aβ1-40 E22Δ dimer

An initial structure calculation with CYANA[28] used only the manually identified 48 unambiguous restraints (Extended Data Table 1) in addition to hydrogen bonds defining the β-sheets (Fig. 3c) and 56 dihedral angle restraints from TALOS+[29]. The resulting backbone structure is shown in Fig. 3b, and a detailed discussion of the calculation procedure is given in the Methods section. A-β is know to form a cross-β fibril with all β-strands poarallel to the fibril axes. Intermolecular restraints (marked in red in Fig. 3b) therefore mark lateral contacts between two given molecules if all β-sheets form a planar arrangement perpendicular to the fibril axis, or as stagger contacts where one monomer spans/extends across two planes[9,30], while intra-molecular restraints (marked in black) are within the same plane to explain the short

distances the represnet. Both assignment possibilities for the intermolecular restraints were explored in the manual structure calculations, but only the all-lateral model fulfills all the manual restraints. The C-terminal hydrophobic residues (Ile32-Val40) do not form a straight β-sheet but fold back such that they fulfill the unambiguously intramolecular contacts Ile32-Met35 (supported by the three peaks marked "M35" in Fig. 2d, and Extended Data Fig. 5c), which clearly do not attenuate upon dilution and are thus intramolecular) and Met35-Gly38 (Extended Data Table 1 and Extended Data Fig. 4e). Further support for this feature, specific to our fold, is provided by the following observations that have not been used in the calculation and thus serve as an independent cross-validation: i) The fold predicts an intramolecular Ile32-Val40 contact (dashed line in Fig. 3b) whose existence is confirmed by the PAR spectrum in Fig. 2d: the signal marked "V40" and assigned to Ile32δ1-Val40γ1/2 is clearly visible and *not* attenuated by dilution. The alternative assignment possibilities for this peak (namely Ile32-Val24 or, with lower probability, Ile32-Val12 or Ile32-Val36) resulted in restraint violations when the corresponding restraint was included into the manual structure calculation. ii) The fold explains all 21 spectrally unambiguous peaks from the [2-^{13}C]-glucose PDSD spectrum listed in Extended Data Table 1, which were not entered into the calculation. These restraints can be added to the manual calculation (using a distance limit of 8.5 Å) and CYANA returns the fold of Fig.3b without restraint violation.

Automatic structure calculation was conducted using in addition to the information from the manual calculation automatically picked peak lists from the CHHC, PAR, PDSD and two PAIN spectra listed in Extended Data Table 2. These peak lists were iteratively assigned by CYANA in the course of the structure calculation (see

Extended Table 2). This procedure yielded the structure shown in Fig. 4, which also fulfills all manually identified unambiguous restraints (Fig. 3a).

The overall organization of the fibril is defined by two interlaced protofilaments (Fig. 4a,c), resembling a cinnamon roll. The different layers are connected by in-register hydrogen bonds leading to the parallel β-sheet form of the fibrillar scaffold. Fig. 4b displays the NMR bundle representing the 20 lowest energy structures with a heavy atom rmsd of 1.1 Å. The cross section of the fibril can be approximated by a rectangle that is closed by intermolecular salt bridges between Glu3 and Lys28 side chains. This salt bridge has not been depicted in wildtype Aβ models, where Lys28 was often found to interact with Asp23[12,30]. Fig. 4c shows the positioning of the side chains in the fibril, and reveals that the very center is filled with exclusively hydrophobic residues, indicating that hydrophobic interactions strongly contribute to fibril stabilty. Interestingly, four charged residues, including the C-terminal carboxylate of Val40, are located inside the fibril core, and form a network of salt-bridged interactions. NMR spectra reveal intermolecular interactions between His13-Val40 (Fig. 1d,e), and intramolecular contacts between His13/His6-Glu11 side chains (Extended Data Fig. 6). This network of salt bridges thus energetically stabilize both the turn region from Gly9 to His13 and the quaternary arrangement of monomers and is another important factor in stabilizing the interior of the fibril.

All calculations discussed above used the MPL of two obtained by STEM. Calculations with MPL equal to three were also performed. They lead to a very similar monomer fold, but also to restraint violations confirming the MPL of two Extended Data Fig. 7).

In conclusion, we present the atomic-resolution structure of a full-length amyloid fibril involved in a human disease. It reveals a new fold not previously observed for amyloids. The structure is highly ordered and its stability can be rationalized with building principles known from other classes of proteins. In contrast to the structural model for the brain-seeded Aβ1-40 fibrils[15], which features a hydrophobic cavity in the center of the fibrils, the Aβ1-40 E22Δ fibrils investigated are tightly packed. Although the structure of Aβ1-40 E22Δ may differ from that of wildtype Aβ fibrils, the deletion mutation does not occur in the central amyloid core region, but at the periphery and is *not* located in a β-sheet where a deletion would invert the in/out pattern of the sidechains and lead to drastic structural changes. Other early-onset Alzheimer related mutants (Arctic, E22G; Dutch, E22Q; Flemish, A21G; Italian, E22K; Iowa, D23N) involve mutations in the very same turn. The overall fold should thus, in principle, also be accessible to the wildtype protein and those mutants. This work provides a structural basis for further investigations on Aβ fibril formation, stability and toxicity, as well as its interaction kinetics and drug binding properties.

Acknowledgement

We thank Alexander Däpp and Andreas Hunkeler for support with the NMR instruments, Prof. Matthias Ernst for expert advice and Beth Lin for help with the STEM measurements and ETH-EMEZ center for help with the TEM. This work has been supported by the Swiss National Science Foundation (grant 200020_134681, 200020_146757), the ETH, the CNRS (ANR-12-BS08-0013-01, ANR-11-BSV8-021-01), and the European Commission under the Seventh Framework Program (FP7;

BioNMR 261863). P.G. is supported by the Lichtenberg program of the Volkswagen Foundation.

Methods Summary

Isotopically labeled Aβ1-40 E22 Δ peptide was expressed recombinantly according to the procedure described in[19]. The peptide spontaneously assembles into amyloid fibrils at physiological salt, temperature and pH conditions (60 μM monomer in 20 mL 10 mM NaH_2PO_4-NaOH pH7.4, 100 mM NaCl, at 37 ˚C, magnetic stirring at 700 rpm, 80 min incubation time). Fibrils were centrifuged into 3.2 mm Bruker NMR rotors at 150'000 g using an ultracentrifuge[31].

NMR spectra were obtained on a Bruker Avance II+ spectrometer operating at a proton frequency of 850 MHz at 19 kHz MAS frequency and were processed with the program Topspin (Bruker Biospin). The data were analyzed using CcpNmr 2.2[32].

Structure calculation was performed with CYANA 3.96 on a decameric (5x2 monomers) segment of the fibril using the Brutus computation cluster of ETH Zurich. While the backbone rmsd of a single bundle was 0.19 Å, the bundle of 20 bundles (calculated using different seed values) had an rmsd of 0.8 Å.

References

1. Hardy, J. & Selkoe, D. The Amyloid Hypothesis of Alzheimer's Disease: Progress and Problems on the Road to Therapeutics. *Science* **297,** 353–356 (2002).
2. Hardy, J. & Higgins, G. Alzheimer's disease: the amyloid cascade hypothesis. *Science* **256,** 184–185 (1992).
3. Tomiyama, T. *et al.* A new amyloid β variant favoring oligomerization in

Alzheimer's-type dementia. *Ann Neurol* **63,** 377–387 (2008).
4. Wasmer, C. *et al.* Amyloid fibrils of the HET-s(218-289) prion form a beta solenoid with a triangular hydrophobic core. *Science* **319,** 1523–1526 (2008).
5. van Melckebeke, H. *et al.* Atomic-resolution three-dimensional structure of HET-s(218-289) amyloid fibrils by solid-state NMR spectroscopy. *J Am Chem Soc* **132,** 13765–13775 (2010).
6. Fitzpatrick, A. W. P. *et al.* Atomic structure and hierarchical assembly of a cross-β amyloid fibril. *P Natl Acad Sci Usa* **110,** 5468–5473 (2013).
7. Tycko, R. & Wickner, R. B. Molecular Structures of Amyloid and Prion Fibrils: Consensus versus Controversy. *Acc Chem Res* **46,** 1487–1496 (2013).
8. Petkova, A. *et al.* A structural model for Alzheimer's beta-amyloid fibrils based on experimental constraints from solid state NMR. *P Natl Acad Sci Usa* **99,** 16742–16747 (2002).
9. Luhrs, T. *et al.* 3D structure of Alzheimer's amyloid-beta(1-42) fibrils. *P Natl Acad Sci Usa* **102,** 17342–17347 (2005).
10. Bertini, I., Gonnelli, L., Luchinat, C., Mao, J. & Nesi, A. A New Structural Model of Aβ40 Fibrils. *J Am Chem Soc* **133,** 16013–16022 (2011).
11. Paravastu, A. K., Leapman, R. D., Yau, W.-M. & Tycko, R. Molecular structural basis for polymorphism in Alzheimer's beta-amyloid fibrils. *P Natl Acad Sci Usa* **105,** 18349–18354 (2008).
12. Ahmed, M. *et al.* Structural conversion of neurotoxic amyloid-β1–42 oligomers to fibrils. *Nat Struct Mol Biol* **17,** 561–567 (2010).
13. Lopez del Amo, J.-M. *et al.* An asymmetric dimer as the basic subunit in Alzheimer's disease amyloid β fibrils. *Angew Chem Int Ed Engl* **51,** 6136–6139 (2012).
14. Petkova, A., Yau, W. & Tycko, R. Experimental Constraints on Quaternary Structure in Alzheimer's -Amyloid Fibrils. *Biochemistry* **45,** 498–512 (2006).
15. Lu, J.-X. *et al.* Molecular Structure of beta-Amyloid Fibrils in Alzheimer's Disease Brain Tissue. *Cell* **154,** 1257–1268 (2013).
16. Pauling, L. & Corey, R. B. Configurations of Polypeptide Chains With Favored Orientations Around Single Bonds: Two New Pleated Sheets. *P Natl Acad Sci Usa* **37,** 729–740 (1951).
17. Guo, J. L. *et al.* Distinct a-Synuclein Strains Differentially Promote Tau Inclusions in Neurons. *Cell* **154,** 103–117 (2013).
18. Bousset, L. *et al.* Structural and functional characterization of two alpha-synuclein strains. *Nature Communications* **4,** 2575 (2013).
19. Ovchinnikova, O. Y., Finder, V. H., Vodopivec, I., Nitsch, R. M. & Glockshuber, R. The Osaka FAD mutation E22Δ leads to the formation of a previously unknown type of amyloid β fibrils and modulates Aβ neurotoxicity. *J Mol Biol* **408,** 780–791 (2011).
20. Inayathullah, M. & Teplow, D. B. Structural dynamics of the ΔE22 (Osaka) familial Alzheimer's disease-linked amyloid β-protein. *Amyloid* **18,** 98–107 (2011).
21. Huber, M. *et al.* Solid-state NMR sequential assignment of Osaka-mutant amyloid-beta (Aβ1−40 E22Δ) fibrils. *Biomol NMR Assign* ahead of print (2014). doi:10.1007/s12104-013-9535-x
22. Wüthrich, K. NMR studies of structure and function of biological macromolecules (Nobel Lecture). *J Biomol NMR* **27,** 13–39 (2003).
23. Lange, A., Luca, S. & Baldus, M. Structural constraints from proton-mediated rare-spin correlation spectroscopy in rotating solids. *J Am Chem Soc* **124,**

9704–9705 (2002).
24. de Paepe, G., Lewandowski, J. R., Loquet, A., Böckmann, A. & Griffin, R. G. Proton assisted recoupling and protein structure determination. *JCP* **129,** 245101 (2008).
25. de Paepe, G. *et al.* Heteronuclear proton assisted recoupling. *JCP* **134,** 095101 (2011).
26. Szeverenyi, N., Sullivan, M. & Maciel, G. Observation of spin exchange by two-dimensional fourier transform 13C cross polarization-magic-angle spinning. *J Magn Reson* **47,** 462–475 (1982).
27. Takegoshi, K., Nakamura, S. & Terao, T. 13C-1H dipolar-driven 13C-13C recoupling without 13C rf irradiation in nuclear magnetic resonance of rotating solids. *J Chem Phys* **118,** 2325–2341 (2003).
28. Guntert, P., Mumenthaler, C. & Wüthrich, K. Torsion angle dynamics for NMR structure calculation with the new program DYANA. *J Mol Biol* **273,** 283–298 (1997).
29. Shen, Y., Delaglio, F., Cornilescu, G. & Bax, A. TALOS+: a hybrid method for predicting protein backbone torsion angles from NMR chemical shifts. *J Biomol NMR* **44,** 213–223 (2009).
30. Tycko, R. Solid-State NMR Studies of Amyloid Fibril Structure. *Annual Review of Physical Chemistry* **62,** 279–299 (2010).
31. Böckmann, A. *et al.* Characterization of different water pools in solid-state NMR protein samples. *J Biomol NMR* **45,** 319–327 (2009).
32. Stevens, T. J. *et al.* A software framework for analysing solid-state MAS NMR data. *J Biomol NMR* **51,** 437–447 (2011).
33. Finder, V. H., Vodopivec, I., Nitsch, R. M. & Glockshuber, R. The recombinant amyloid-beta peptide Abeta1-42 aggregates faster and is more neurotoxic than synthetic Abeta1-42. *J Mol Biol* **396,** 9–18 (2010).
34. Lin, Y. J., Kirchner, D. K. & Guntert, P. Influence of 1H chemical shift assignments of the interface residues on structure determinations of homodimeric proteins. *J Magn Reson* (2012).

Figure captions:

Fig. 1. a Negative stain TEM micrograph of Aβ1-40 E22Δ fibrils. **b** STEM micrograph of unstained, freeze-dried fibrils. Regions used for mass-per-length measurements are marked in red. **c** MPL measurement: the basic filament unit is a dimer (two monomers per layer of β-sheet). The comparison of NCO (**d**) and NCA (**e**) NMR spectra of uniformly [^{15}N,^{13}C]-labeled fibrils (black contours) with PAIN spectra of 1:1 mixed [^{15}N]:[^{13}C]-labeled fibrils (orange contours) establishes an in-register parallel β-sheet architecture. Additional intermolecular long-range contacts are labeled in red. **e,f** Trace taken at the Gln15 Nε2-resonance from PAIN spectra a 1:1 mixed [^{15}N]:[^{13}C]-labeled sample (d,e). For the intermolecular peaks in the orange spectrum, the peaks marked Q15 mark a rough distance

calibration of about 4.8 Å, as they are register peaks with the ^{15}N and ^{13}C spins in adjacent β-strands. Peaks stronger than these register peaks are indicative of even shorter distances.

Fig. 2. Extracts of NMR spectra that distinguish intra- from intermolecular contacts. **a,b** Overlay of PAR spectra recorded on a uniformly [^{13}C]-labeled sample (black contours) and on a dilutely labeled sample composed of 20% uniformly [^{15}N,^{13}C]-labeled protein and 80% unlabeled material (green contours). Signal attenuation due to dilution of intermolecular contacts is observed for the peaks labeled in red. **c** Intensity ratios of unambiguous long-range cross peaks recorded on the dilutely labeled sample versus those recorded on uniformly labeled sample. Inter- and intramolecular correlations, expected to be attenuated to 20% and not attenuated, are shown as red and black columns, respectively. The full statistics are shown in Extended Data Fig. 4. **d** Trace taken at the Ile 32 Cδ1-resonance from PAR spectra of uniformly (black) versus dilutely labeled (green) samples. All cross peaks of this resonance are intramolecular.

Fig. 3. **a** Interaction matrix with spectrally unambiguous inter- and intramolecular contacts indicated in red and black, respectively. Blue contacts do not lead to spectrally unambiguous cross-peaks and are therefore not used for the manual structure calculation, but they allow to cross-check the structure. **b** Backbone model of Aβ1-40 E22Δ calculated on the basis of unambiguous distance restraints (solid red and black lines). Blue dashed contacts are discussed in the main text but were not used in the calculation. **c** Register hydrogen bonds between β-strands entered into the calculation (green lettering).

Fig. 4. Representation of the atomic-resolution structure of Aβ1-40 E22Δ calculated from NMR-derived distance and torsion-angle restraints. **a** Schematic view of the lowest-energy conformer of a Aβ1-40 E22Δ bi-decamer (2x10 monomers). The symmetry axis coincides with the long axis of the fibril and is indicated by a black arrow. **b** NMR bundle: The backbone rmsd (all heavy atom rmsd) amounts to 0.8 (1.1). Only the central dimer of a five-layered fibril is shown. **c** Cross section of the fibril (lowest-energy structure from b). Hydrophobic residues are colored white, negatively charged residues red, positively charged residues blue, and polar ones (and Gly) green.

Methods

Protein expression and purification

Plasmid construction for recombinant expression of Aβ1-40 E22Δ in E. coli as well as protein expression, purification and fibril production have been described in detail[19,33]. The protein monomer concentration used here for fibrillization was 60 μM, in a reaction buffer of 10 mM NaH_2PO_4-NaOH pH 7.4, 100 mM NaCl, at 37 °C, 700 rpm magnetic stirring, 80 min incubation time.

Mass per length measurements using STEM

An aliquot of the fibrillization mixture was taken after 90 min and immediately washed using ammonium acetate buffer, blotted onto custom-made EM grids and freeze-dried. The remaining fibrils were washed and ultracentrifuged. The NMR spectrum of this sample was identical to the one shown in Extended Data Fig. 1, demonstrating that the fibrils used in STEM measurements are identical to fibrils used for NMR spectroscopy.

STEM measurements were carried out at Brookhaven National lab. STEM data were analyzed using PCMass32 (http://www.bnl.gov/biology/stem/). . The criteria for manual selection of filaments were that filaments were straight and regular in appearance, not fragmented, well-isolated, with a clean background and not embedded in salt, monomer or denatured protein. 159 manual mass measurements were conducted and a histogram is shown in Fig. 1c.

NMR structure determination

Sample preparation

The fibrils were centrifuged for 45 min at 30,000 g and 4 °C, washed with deionized water and centrifuged again. The pellet containing approximately 10-15 mg Aβ1-40 E22Δ fibrils was resuspended in 800 μL deionized water and packed into a 3.2 mm ZrO_2 rotor (Bruker Biospin) using ultracentrifugation and a home-made filling device[31], at 150.000 g for 16 hours.

Data recording

All NMR spectra were recorded on a Bruker Avance II+ at a static magnetic field of 20.0 T using a Bruker 3.2 mm triple-resonance probe spinning at 19 kHz (except for the PDSD spectrum of the [2-^{13}C glucose]-labeled sample, which was recorded at 11.5 kHz MAS). Sample temperatures were 5-15° C as determined from the water resonance position[31]. A list of the NMR experiments recorded on various samples and the corresponding experimental parameters are listed in Extended Data Table 3. The spectra of the uniformly [^{15}N,^{13}C]-labeled sample were referenced to DSS and the shifts of all other samples were referenced to this sample. All spectra were processed in TopSpin 2.1 (Bruker Biospin). Spectra were zero-filled to the next power of two in data points. Spectra used for dilution analysis were zero-filled, before Fourier transform, to 16k x 16k data points.

Analysis of the spectra

Spectra were analyzed and annotated using CcpNmr version 2.2.2[32]. To account for small chemical shift variations between fibril batches, separate shift lists were maintained for every sample. For CHHC assignment, ^{13}C shifts were translated to ^{1}H assignments of the closest proton (in terms of number of bonds separating ^{13}C and ^{1}H).

Hydrogen-bond restraints were identified when three consecutive negative secondary chemical shifts were observed[21] with the exception of Glycine residues, for which no β-strands were imposed. Their position is indicated in Fig. 3c. Dihedral angle restraints were predicted from the ^{13}C and ^{15}N chemical shifts using the TALOS+[29] and only predictions rated as "good" were used. Almost all Glycines produced TALOS+ warnings and all Gly residues were excluded from the torsion-angle restraints.

For manual restraint identification, isolated correlations that could be spectrally unambiguously assigned to single resonances in both dimensions within a tolerance of 0.2 ppm were identified in the following spectra (and samples): DARR 400 ms, PAR 8 ms, CHHC 500 us (U-[^{13}C]-labeled and dilutely labeled), PAIN 6 ms (U-[^{15}N,^{13}C]- and mixed [^{15}N]:[^{13}C]-labeled) and PDSD 4 s ([^{15}N, 2-^{13}C glucose]-labeled). PAIN peaks in the mixed sampel are automatically intermolecular. Signal-to-noise ratio permitting, the remaining restraints were subjected to further analysis in order to identify their inter- or intramolecular nature. To this purpose, the spectrally

unambiguous peaks identified in DARR 400 ms, PAR 8 ms, CHHC 500 µs (U-[^{13}C]) were compared to the equivalent spectra recorded on the dilutely labeled sample. Example traces are shown in Extended Data Figure 4. Great care was taken to normalize the intensities for each residue using intramolecular peaks free of spectral overlap and to adjust the position of the two traces such that they are at the peak maximum. The intensity ratios of peak maxima I_{dil}/I_{uni} were evaluated and the detailed results are displayed in Extended Data Figure 5 and a per residue averages are summarized in Fig. 2c. Errors were estimated from the noise level and represent standard deviations. Peaks were subsequently classified as intramolecular if the intensity ratio was $I_{dil}/I_{uni} \geq 0.8$ with a lower error margin above 0.4. Conversely, peaks were classified as intermolecular if $I_{dil}/I_{uni} \leq 0.4$ with an upper error margin below 0.8. In all other cases no classification was done. The corresponding restraints were translated to upper distance restraints with distances values listed in Extended Data Table 2. This data analysis yield in a list of unambiguous restraints, spectrally as well as with respect to intra-/intermolecular as listed in Extended Data Table 1.

Optimal upper distance limits for each experiment were determined following the L-curve approach[5]. The optimum distances found are given in Extended Data Table 2 and they are very similar to the ones in[5].

Peak lists for automatic structure calculation were generated using automatic peak picking performed in CcpNmr. Spinning-sideband positions were removed manually.

Structure calculation

Structure calculation was performed in CYANA 3.96. All manual and automatic restraints were given the same relative weight (1.0) except for hydrogen-bond upper and lower distance limits (relative weight 10.0). Hydrogen bonds were implemented as lower and upper distance limits from H^N and N to O of 1.8-2.0 Å and 2.7-3.0 Å, respectively. Fibril structure calculation was performed for a penta-dimer (5x2 monomers), tri-dimer (3x2) or deca-dimer (10x2). No significant differences were detected, as expected[5]. For comparison tri-trimers (3x3) and pentatrimers were calculated. Symmetry was enforced for all molecules by minimizing dihedral angle-

differences and differences in restrained interatomic distances between the monomers[34]. Restraint assignment in the automatic calculation was allowed between all monomers and assignments were enforced to be C2(C3)-symmetric with respect the fibril long axis. His6 and His13 were implemented as positively charged as indicated by the sidechain nitrogen chemical shifts. The N-terminal aspartate and the C-terminal valine residue were treated as positively and negatively charged, respectively.

The following restraints were used for **manual structure calculation** (numbers are given per monomer): 31 manual restraints (upl) supported by the 48 unambiguous cross peaks listed in Extended Data Table 1 with 15 intermolecular upl's entered as either staggered or lateral, 28 pairs of ϕ/ψ dihedral angle restraints for the residues in green or blue lettering in Fig 3c; 19 hydrogen bonds between residues in green lettering in Fig. 3c. Upper distance restraints of 5.0, 6.0, 6.0 and 7.0 Å were applied for restraints from CHHC, PAR, PAIN and DARR spectra. 1000 structures were annealed in 35,000 torsion-angle dynamics steps. The structure with the lowest target function (0.1 per monomer) had no violations and is shown in Fig. 3b. All 16 permutations of the possible relative direction of the five β-sheets were evaluated in separate CYANA structure calculations. Only a single arrangement of β-sheets yielded a violation-free solution. This solution represents a planar arrangement with all intermolecular restraints fulfilled within the plane of Fig. 3b. Attempts to use staggered arrangements to fulfill the restraints by alternative motifs always lead to violations. This observation is in line with the existence of a significNT number of intramolecular restraints along the entire sequence (black lines in Fig.3b), which are impossible to fulfill if the molecule is not contained in a single plane.

For **automatic** structure calculation the same input as for manual structure calculation was used. In addition, restraints from five spectra were automatically assigned by CYANA: peak lists of the PAR 8 ms, CHHC 500 μs, and PDSD 4 s, two PAIN 6 ms spectra (with the ^{13}C carrier on aliphatic and on aromatic resonances during the PAIN transfer) using chemical-shift lists of the respective samples. For the final calculations, additional restraints for salt bridges were generated for oppositely charged residues for which ^{13}C-^{13}C or ^{13}C-^{15}N side chain contacts were observed in the spectra. Upper limit restraints were introduced for Glu3 Oε1/2 to Lys27 Nζ (5 Å); His6 Nε2 to

Glu11Oε1/2 to (4 Å); Glu11Oε1/2 to His13 Nε2 (4 Å); His13 Nδ1 (4 Å) to Val40 O1/2. (Extended Data Fig. 7). 500 structures were annealed in 35,000 steps in seven assignment cycles. Again all 16 relative orientations of the 5 β-sheets were calculated and the one which fulfilled all manual restraints was again the one with by far the lowest target function for the automatic calculation..

For the width of the NMR bundle, we used a measure that also considers the random seed-dependence of the CYANA calculation and we construct a bundle of the best structure from 20 different bundles each calculated from a different "random" initial condition determined by the initial "seed" value of CYANA. This bundle is deposited in the PDB protein data databank (http://www.rcsb.org) under the ID XXXX). While the backbone rmsd of a single bundle was 0.2 ± 0.1 Å, the bundle of 20 bundles had an rmsd of 0.8 ± 0.3 Å. The heavy atom rmsd were 0.6 ± 0.1 Å and 1.1 ± 0.3 Å, respectively. Variations between the bundles can result from different assignments options that have been chosen for highly ambiguous cross peaks in different CYANA runs.

Out of all 20 bundles, the structure with the lowest CYANA target function is shown in Fig. 4. In the best structure out of 500 structures, residues were distributed as follows: most favored 82.5%, 14.3% additionally allowed, 3.2% generously allowed, 0% disallowed.

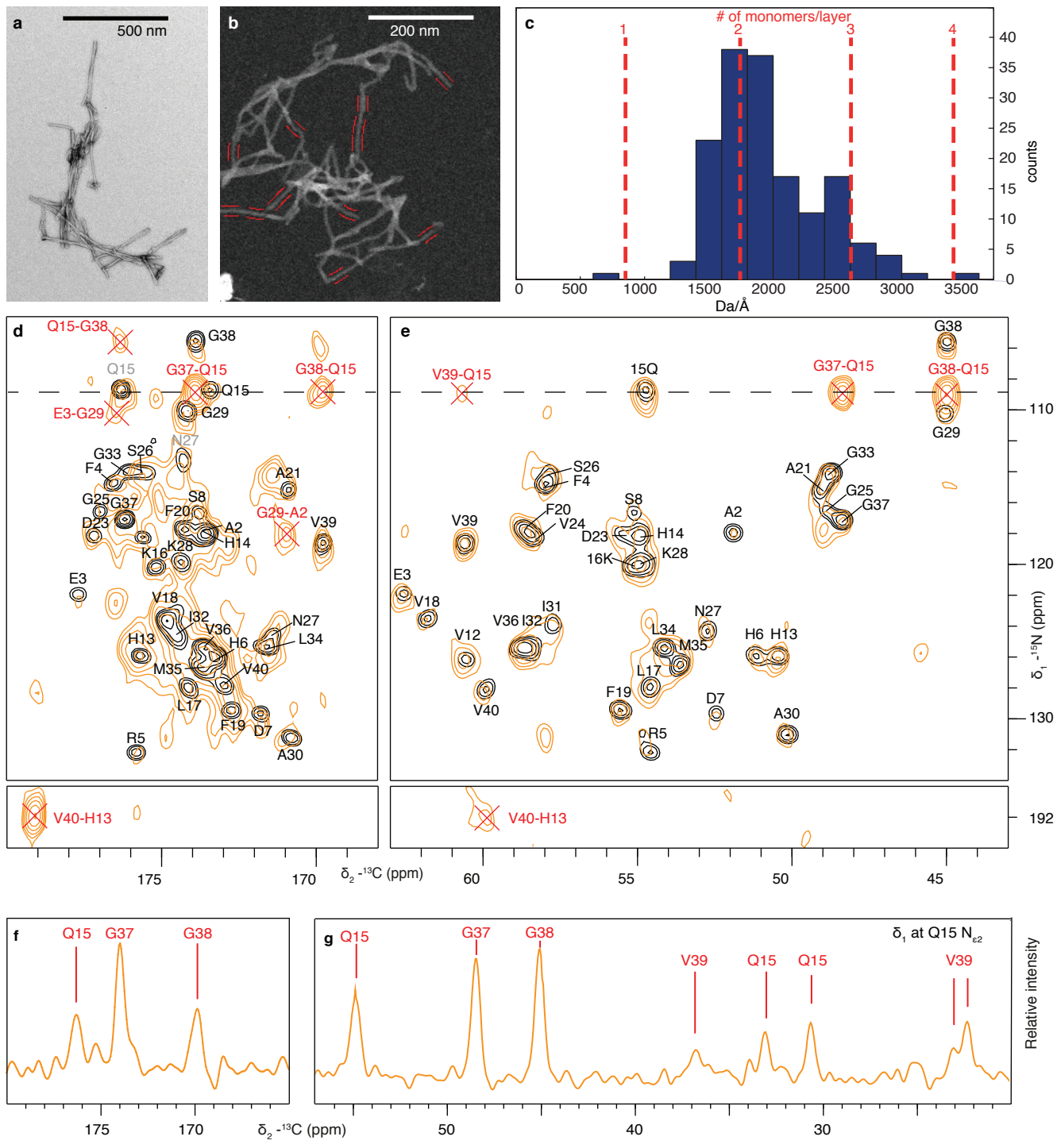

a
500 nm
b
200 nm
c
# of monomers/layer
1
2
3
4
counts
Da/Å
d
Q15-G38
G38
Q15
G37-Q15
G38-Q15
E3-G29
G29
N27
G33
S26
F4
A21
G25
G37
S8
F20
G29-A2
V39
D23
A2
H14
K16
K28
E3
V18
I32
V36
N27
H13
H6
L34
M35
V40
L17
F19
D7
R5
A30
V40-H13
e
V39-Q15
15Q
G37-Q15
G38-Q15
G38
G29
S26
F4
G33
A21
G25
G37
S8
F20
V24
V39
D23
H14
A2
16K
K28
E3
V18
I31
V36
I32
N27
V12
L34
M35
H6
H13
L17
F19
D7
V40
A30
R5
V40-H13
δ2 -13C (ppm)
δ1 -15N (ppm)
f
Q15
G37
G38
g
Q15
G37
G38
δ1 at Q15 Nε2
V39
Q15
Q15
V39
Relative intensity
δ2 -13C (ppm)

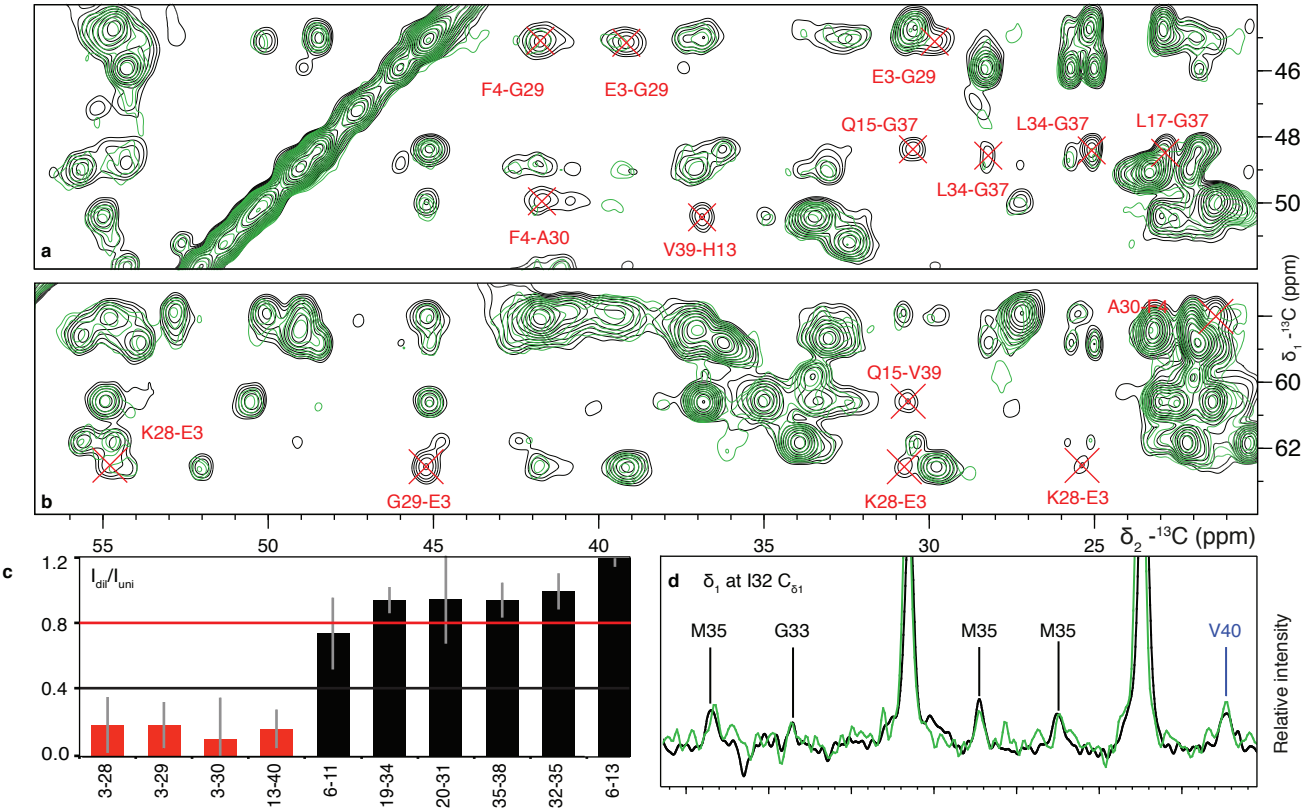
a
F4-G29
E3-G29
E3-G29
Q15-G37
L34-G37
L17-G37
L34-G37
F4-A30
V39-H13
46
48
50
b
A30-F4
Q15-V39
K28-E3
G29-E3
K28-E3
K28-E3
60
62
δ1 -13C (ppm)
55
50
45
40
35
30
25
δ2 -13C (ppm)
c
Idif/Iuni
1.2
0.8
0.4
0.0
3-28
3-29
3-30
13-40
6-11
19-34
20-31
35-38
32-35
6-13
d
δ1 at I32 Cδ1
M35
G33
M35
M35
V40
Relative intensity

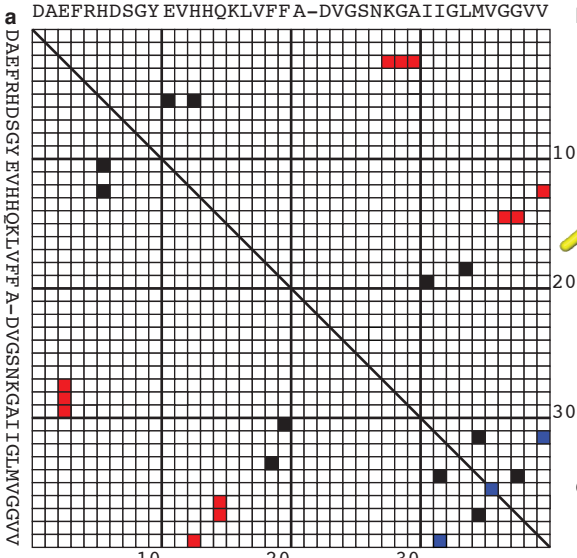
a
DAEFRHDSGY EVHHQKLVFF A-DVGSNKGAIIGLMVGGVV
DAEFRHDSGY EVHHQKLVFF A-DVGSNKGAIIGLMVGGVV
10
20
30
10
20
30

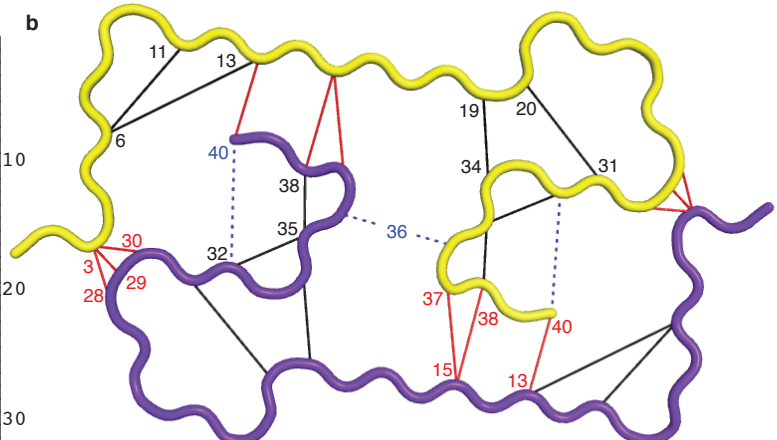
b
11
13
6
40
38
35
32
30
3
28
29
19
20
34
31
36
37
38
40
15
13

c
10
20
30
40
DAEFRHDSGYEVHHQKLVFFA-DVGSNKGAIIGLMVGGVV
β1
β2
β3
β4
β5

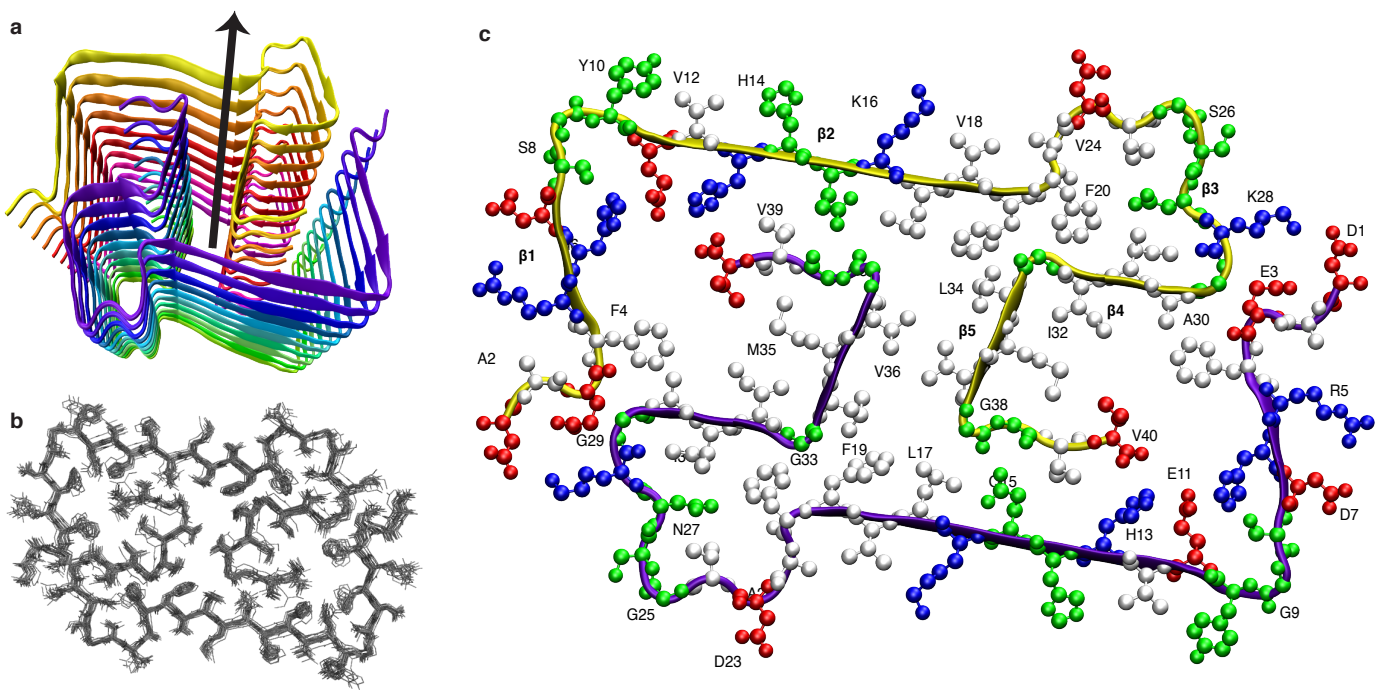
a
b
c
Y10
V12
H14
K16
V18
S26
S8
β2
V24
F20
β3
K28
V39
D1
β1
E3
L34
β4
A30
F4
β5
I32
M35
A2
V36
R5
G38
G29
V40
G33
F19
L17
E11
N27
H13
D7
G25
G9
D23